

APPENDIX J Surface-Based Geophysical Survey Report



**GEOPHYSICAL REPORT
SURFACE GEOPHYSICAL SURVEY**

**Last Chance Grade Project
PA&ED Phase B2
Del Norte County, California**

GEOVision Project No. 20020

Prepared for

Kleinfelder

2882 Prospect Park Drive, Suite 200

Rancho Cordova, CA 95670

Prepared by

GEOVision Geophysical Services, Inc.

1124 Olympic Drive

Corona, CA 92881

(951) 549-1234

March 12, 2021

Report 20020-01 Rev 1

Report 20020-01 REVISION HISTORY

DATE	REVISION NUMBER	REASON FOR CHANGE
2/10/2021	0	Draft Issue
3/12/2021	1	Incorporates Kleinfelder draft boring logs and GEOVision draft borehole results

TABLE OF CONTENTS

1	INTRODUCTION	1
2	METHODOLOGY	2
2.1	SEISMIC REFRACTION INVESTIGATION.....	2
2.2	ELECTRICAL RESISTIVITY INVESTIGATION.....	3
3	EQUIPMENT AND FIELD PROCEDURES.....	4
3.1	SURVEY CONTROL.....	4
3.2	SEISMIC REFRACTION SURVEY.....	4
3.3	ELECTRICAL RESISTIVITY SURVEY.....	5
4	DATA REDUCTION AND MODELING	6
4.1	SEISMIC REFRACTION.....	6
4.2	ELECTRICAL RESISTIVITY IMAGING.....	7
5	DISCUSSION OF RESULTS.....	9
5.1	SEISMIC REFRACTION LINE SL-41	9
5.2	SEISMIC REFRACTION LINE SL-42	10
5.3	SEISMIC REFRACTION AND RESISTIVITY LINE SL-43	10
5.4	SEISMIC REFRACTION LINE SL-11	11
5.5	SEISMIC REFRACTION LINE SL-12.....	11
5.6	SEISMIC REFRACTION LINE SL-13A	11
5.7	SEISMIC REFRACTION LINE SL-13B	12
5.8	SEISMIC REFRACTION LINE SL-20	13
5.9	SEISMIC REFRACTION LINE SL-17	13
5.10	LANDSLIDE INTERPRETATION.....	14
6	CERTIFICATION	15
7	REFERENCES	16
8	TABLES AND FIGURES.....	17

LIST OF TABLES

Table 1 Geophysical Line Geometry

LIST OF FIGURES

Figure 1 Site Location Map
Figure 2 Site Map (SL-41, 42, 43)
Figure 3 Site Map (SL-11, 12, 13A, 13B)
Figure 4 Site Map (SL-17, 20)
Figure 5 Line SL-41 Seismic Refraction Model
Figure 6 Line SL-42 Seismic Refraction Model
Figure 7 Line SL-43 Seismic and Electrical Resistivity Models
Figure 8 Line SL-11 Seismic Refraction Model
Figure 9 Line SL-12 Seismic Refraction Model
Figure 10 Line SL-13A Seismic Refraction Model
Figure 11 Line SL-13B Seismic Refraction Model
Figure 12 Line SL-20 Seismic Refraction Model
Figure 13 Line SL-17 Seismic Refraction Model

1 INTRODUCTION

A geophysical survey was conducted in Del Norte County, California on January 14-20 of 2021. This work was conducted under HNTB Project Number 71188, Contract Number 03A2996, Last Chance Grade PA&ED Phase, Phase Order B2. The **GEOVision** reference project number is 20020.

The geophysical survey consisted of nine seismic refraction lines and a single electrical resistivity line, as shown in Figures 1, and in more detail on Figures 2-4. Lines SL-41, SL-42, and SL-43 were conducted on the California Department of Transportation (Caltrans) right of way for Highway 101. Lines SL-11, SL-12, SL-13A, SL-13B and SL-17 were located within Redwood National Park and Del Norte Coast Redwoods State Park. SL-20 was located on private property. The endpoints of each geophysical line were surveyed by **GEOVision** personnel using a real-time differential global positioning system. Coordinates are provided in Table 1.

The geology in the vicinity of SL-17 was expected to consist broken formations of Early Cretaceous and Late Jurassic rocks, including massive greywacke sandstone, and interbedded sandstone, mudstone, and conglomerate (Delattre and Rosinski, 2012). SL-20 is over rocks mapped as Mélange unit of Crescent City, which can include metasedimentary rocks as well as marine sedimentary rocks. Lines SL-11, SL-12, SL-13A, SL13B, SL-41, SL-42, and SL-43 are either over this Mélange or Quaternary landslide deposits with primarily west-southwest direction of movement (Wills, 2000).

The following sections include a discussion of methodology, equipment and field procedures, data reduction and modeling, and results of the geophysical survey.

2 METHODOLOGY

2.1 *Seismic Refraction Investigation*

Detailed discussions of the seismic refraction method can be found in Lankston (1990), Telford et al. (1990), Dobrin and Savit (1988), and Redpath (1973). When conducting a seismic survey, acoustic energy is input to the subsurface by an energy source such as a sledgehammer impacting a metallic plate, weight drop, vibratory source, or explosive charge. The acoustic waves propagate into the subsurface at a velocity dependent upon the elastic properties of the material through which they travel. When the waves reach an interface where the density or velocity changes significantly, a portion of the energy is reflected back to the surface and the remainder is transmitted into the lower layer. Where the velocity of the lower layer is higher than that of the upper layer, a portion of the energy is also critically refracted along the interface. Critically refracted waves travel along the interface at the velocity of the lower layer and continually refract energy back to the surface. Receivers (geophones) laid out in linear array on the surface record the incoming refracted and reflected waves. The seismic refraction method involves analysis of the travel times of the first energy to arrive at the geophones. These first arrivals are from either the direct wave (at geophones close to the source) or critically refracted waves (at geophones further from the source).

Errors in seismic refraction models can be caused by velocity inversions, hidden layers, or lateral velocity variations. At sites with steeply dipping or highly irregular bedrock surfaces, refractions from structures to the side of the line rather than from beneath the line may severely complicate modeling. A velocity inversion is a geologic layer with a lower seismic velocity than an overlying layer. Critical refraction does not occur along such a layer because velocity has to increase with depth for critical refraction to occur. This type of layer, therefore, cannot be recognized or modeled and depths to underlying layers would be overestimated.

A hidden layer is a layer with a velocity increase, but of sufficiently small thickness relative to the velocities of overlying and underlying layers, that refracted arrivals do not arrive at the geophones before those from the deeper, higher velocity layer. Because the seismic refraction method generally only involves the interpretation of first arrivals, a hidden layer cannot be recognized or modeled and depths to underlying layers would be underestimated. Saturated sediments overlying high velocity bedrock can be a hidden layer under many field conditions. Generally, saturated sediments have a much higher velocity than unsaturated sediments, typically in the 5,000 to 7,000 ft/s range and can occasionally be interpreted as a second arrival when the layer does not give rise to a first arrival.

A subsurface velocity structure that increases as a function of depth rather than as discrete layers will cause depths to subsurface refractors to be underestimated in a manner very similar to that of the hidden layer problem. Lateral velocity variations that are not adequately addressed in the seismic models also lead to depth errors. Tomographic imaging techniques can often resolve the complex velocity structures associated with hidden layers, velocity gradients, and lateral velocity variations. However, in the event of an abrupt increase in velocity at a geologic horizon, the velocity model generated using tomographic inversion routines will smooth the horizon with velocity possibly being underestimated at the interface and overestimated at depth.

2.2 Electrical Resistivity Investigation

Electrical resistivity tomography (ERT) involves the measurement of the apparent resistivity of subsurface soil and rock as a function of depth and/or position. The ERT method can identify variations in subsurface geologic features where contrasts in the resistivities are present. Changes in the electrical properties of the subsurface are non-unique indicators of geologic conditions (Dahlin, 1996). Variations in subsurface moisture content, porosity, permeability, and soil or rock type (i.e., lithology) affect electrical resistivity measurements. Cultural features (man-made features such as fences, power lines, pipelines, and buried debris) can influence resistivity measurements.

During a resistivity survey, electrical current is applied to a pair of electrodes (a dipole), and the potential difference (voltage) is measured between one or more pairs of potential electrodes. For a 2-D resistivity survey, the current and potential electrodes are generally arranged in a linear array. Common array types include pole-pole, dipole-dipole, Schlumberger, Wenner, and gradient arrays. The apparent resistivity is the resistivity of a homogenous and isotropic half-space that would yield the measured resistivity for a given input current and potential difference for a given arrangement of electrodes. It is calculated by dividing the measured potential difference by the input current and multiplying by a geometric factor calculated for the array.

Apparent resistivity is typically run through an inverse modeling algorithm to generate a geoelectric section of the subsurface directly beneath the profile (Loke and Barker, 1996). The inversion process involves creating a hypothetical earth model of cells with infinite length perpendicular to the line, calculating the theoretical resistivity of this model, and iteratively adjusting the resistivity of the cells to minimize error between the calculated and observed resistivity. The final result of the inversion process is a resistivity model of the subsurface that fits the observed data with input error and smoothness constraints.

Depth of investigation for the ERT method is a complex function involving receiver array length and the electrical properties of the subsurface materials (Oldenburg and Li, 1999). In general, for 2D electrical resistivity surveys, resolution and depth of investigation are inversely proportional. High resolution is typically obtained by using relatively small electrode spacing. However, using small electrode spacing reduces investigation depth. Conversely, large electrode separation will typically provide greater depth of investigation but sacrifices resolution.

3 EQUIPMENT AND FIELD PROCEDURES

3.1 Survey Control

The geophysical traverses were communicated to **GEOVision** by Mr. Eric Wilson of Caltrans. General line clearing had been performed by another party. Receiver (geophone and electrode) locations for the seismic refraction and electrical resistivity lines were marked using a 300 ft tape measure, typically by establishing the beginning of the line at a survey stake labeled “South End” by others. A Trimble R10 GPS system with CenterPoint RTX real-time corrections was used to occupy line endpoints, and most receiver locations collected along the survey lines. All GPS data was transferred to a spreadsheet including receiver ID, Easting, Northing (State Plane Coordinate System, California Zone 1, North American Datum of 1983, US feet for units) and elevation (North American Vertical Datum of 1988, Geoid 12B, US feet for units). Elevations along the refraction lines were surveyed using the Trimble R10 GPS in open areas and a Nikon NK-7 auto level and 25-foot survey rod where GPS coverage was poor.

The locations of the geophysical traverses are shown on Figures 1-4 and the coordinates for the endpoints of each line are summarized in Table 1. All of the lines within the trees are presented as “approximate” due to tree canopy degrading GPS data quality. The electrical resistivity line along SL-43 was set up to “start” coincident with the seismic refraction line, but line lengths vary slightly between the methods depending on individual spread lengths and recording parameters.

3.2 Seismic Refraction Survey

Seismic refraction equipment used during this investigation consisted of two Geometrics Geode 24-channel signal enhancement seismographs (to record up to 48 live channels), 4.5 Hz vertical geophones with Kooter-style takeouts, seismic cables with ~13-foot takeouts, piezo hammer switches, a Betsy Seisgun loaded with electrically-primed seismic ammunition, a 20-lb. sledgehammer, a 40-kg accelerated weight drop, and an aluminum strike plate.

Geophone spacing for this investigation was 4 to 10 feet. The number of geophones and total length per line are outlined in Table 1.

A minimum of 10 shot points were acquired per spread to facilitate tomographic modeling (described below). Shot points included off-end shots (where possible), end shots, and multiple interior shot points. Space, access, and topography limited or prohibited the placement of some off-end shots.

A hammer switch was used to trigger the seismograph upon impact. The final seismic record at each hammer shot point was the result of stacking 7 to 20 shots to increase the signal to noise ratio; shot points using the Betsy Seisgun were not stacked. All seismic records were stored on a laptop computer. Data acquisition parameters, file names, and other observations were recorded on a digital observer’s log, which is retained in project files.

3.3 Electrical Resistivity Survey

ERT equipment used during this investigation consisted of an Advanced Geosciences, Inc. Supersting R8/IP transceiver, 18-inch stainless-steel electrode stakes, and sealed multi-core electrode cables takeouts. The 400-volt transmitter is capable of output current levels of 2-amperes at 200 watts. It was powered by 12V sealed AGM batteries. The instrument can record up to eight channels simultaneously and switching between up to 112 electrode pairs to act as current or potential dipoles.

Resistivity line SL-43 consisted of electrodes spaced 10 feet apart. The geophone locations from the seismic refraction survey were used for electrode locations. The electrodes were driven into the ground approximately 12 inches (or more). Each electrode was connected to the multicore electrode cable via a steel spring or rubber band to create electrical coupling between the metal electrode stake and metal cable takeout.

A contact resistance test was performed to monitor the resistance values between each pair of electrodes. Dipoles with anomalously high contact resistances were checked (ensuring adequate coupling of the electrode to the soil and verifying clean metal-metal contact between the multicore cable and electrode) and the contact resistance test repeated. If anomalously high contact resistance readings persisted, the electrode location was adjusted and the test repeated. Soils along SL-43 were very saturated, contact resistance values were reasonably low, and a salt-water solution was not applied to the electrodes.

Operation of the AGI Supersting was partially automated. Prior to taking measurements, a sequence file was loaded to the instrument. This file specifies which pairs of electrodes to function as the current dipole, and which pairs of electrodes to act as potential difference dipoles for each measurement. The instrument read this sequence file and commenced with the automatic data collection. For each line of the sequence, multiple measurements were performed and the standard deviation between those measurements was calculated. If that standard deviation value exceeded a percentage programmed by the operator (for this project, 3%), that measurement was repeated up to two times. If the standard deviation after two repeats did not improve below the programmed threshold, the reading was stored and flagged for later evaluation during data processing. Typically, the standard deviation was within the 3% threshold, and the instrument stored the reading and advanced to the next line of the sequence file.

During the measurement cycle, the instrument displayed the sequence number, current applied, voltage differential recorded at each dipole, and the standard deviation between repeat measurements. The operator monitored these values for anomalously low current values, negative recorded voltages, and high standard deviation values that may indicate potential problems for the geophysical survey. If a problem was identified during data collection, the operator paused the measurement cycle and inspected the electrode array for problems such as loose electrodes, disconnected electrodes, or nearby cultural features that may impact the recorded apparent resistivity values. If no obvious sources of error were noted, the operator made note in the data recording log for evaluation during data processing.

4 DATA REDUCTION AND MODELING

4.1 *Seismic Refraction*

The first step in data processing consisted of picking the arrival time of the first energy received at each geophone (first arrival) for each shot point. The first arrivals on each seismic record are either a direct arrival from a wave traveling in the uppermost layer, the air-wave or a refracted arrival from a subsurface interface where there is a velocity increase. First-arrival times were selected using the manual picking routines in the SeisImager™ software suite (Geometrics, Inc., v5.8.02). So-called “autopickers” were not used. These first-arrival times were saved in an ASCII file containing shot location, geophone locations, and associated first-arrival time. Errors in the first-arrival times were variable with error generally increasing with distance from the shot point, especially where data quality was affected by wave action, construction activities, and traffic noise. Noise levels were significant. Given the proximity to noise sources, the signal to noise levels for geophones far from the energy source was often poor. First-arrival times were not picked when the processor felt the noise could be obscuring the first arrival or the picks may be suspect. When possible to pick reliably and consistently, the processing geophysicist picked “around” the air-wave, in an attempt to better characterize the soil velocity of the shallowest layer, and improve the depth estimates for subsequent layers.

Analysis of seismic refraction data depends upon the complexity of the subsurface velocity structure. Layer-based and tomographic inversion routines can be used to model the seismic data. Layer-based methods are better suited when subsurface units are arranged along distinct geologic boundaries, whereas tomographic methods may be better applied when gradational changes across geologic contacts. These different modeling schemes have their own strengths and weaknesses. Layer-based modeling is best suited when clearly defined, homogenous units are observed in the raw data and describe the geology. In other words, this method performs better when layer-cake geology or hard contacts are present in the subsurface. It is also useful for mapping the groundwater table within soft sediments (P-wave refraction). Tomographic inversion is better suited when vertical and lateral velocity gradients are observed in raw field data and verified by the travel-time curves (Ali, 1990; Rohdewald, 2011). This is common with thick sequences of unconsolidated sediments that are increasing with velocity due to compression at depth, weathering zones, or strong lateral changes in the bedrock profile. However, tomographic modeling methods force a velocity gradient across apparent geologic units or vertical cross-section, smoothing the velocity ranges presented in the model. Typically, this will result in an apparently slower seismic velocity at the layer contact compared to the layer-based model.

Seismic refraction data were first modeled using a two or three-layer modeling algorithm to fit the major trends in the travel time data. This layer-based model was then used as a starting model for tomographic inversion as available in the SeisImager and Rayfract® (Intelligent Resources, Inc. v4.01) software packages. Refraction tomography techniques are often able to resolve complex velocity structure (e.g., velocity gradients) that can be observed in bedrock weathering profiles. Layer-based modeling techniques such as GRM are not able to accurately model the velocity gradients that can be observed in weathered or transitional zones. However, tomographic modeling methods force a velocity gradient across apparent geologic units or

vertical cross-section, smoothing the velocity ranges presented in the model. Typically, this will result in an apparently slower seismic velocity at the contact compared to the layer-based model. The final tomographic velocity models for the seismic line were exported as ASCII files and imported into the Golden Software Surfer v19 mapping system where the velocity model was gridded, contoured, and annotated for presentation.

4.2 Electrical Resistivity Imaging

Raw resistivity data were first evaluated in *pseudosection* format (i.e., station versus “n” spacing). Note that pseudo-sections are not cross-sections or earth models as the dipole-dipole pseudosection plotting method is not a depth representation (Edwards, 1977), but it is a useful means of evaluating data graphically. The pseudosection was analyzed for individual data points with high reported error (RMS error between measurements). Data with extremely high (>10%) variance between measurements were automatically discarded. Points interpreted as outliers beyond the trends observed in the geophysical data as expected for the geologic environment, were manually evaluated and removed. Due to physical and geometric constraints, a single spurious point would not represent an accurate apparent resistivity value for a measurement point. These spurious points can be identified on the raw pseudosections and removed. This does not include all outlier data. For example, if a zone of anomalously high apparent resistivity values is observed in the data, those points would not be removed prior to inversion. Other data points with lower error were discarded if they did not appear to match the geoelectric section – a spurious high resistivity value surrounded by conductive measurements, for example. When patterns of “noisy” data were determined to be associated with a single electrode location, all data associated with that electrode location was reviewed in greater detail. It is uncommon, but possible, for an electrode to become unplugged after preliminary testing but during data collection, and all subsequent data collected using that electrode to be in error.

After data processing, the averaged apparent resistivity data were input into EarthImager2D (AGI) for two-dimensional modeling. An ASCII formatted station file summarizing the electrode geometry, project stationing, and elevation is imported prior to inversion. The final model cross-sections for the ERT survey are derived from smooth-model inversion results of the dipole-dipole data. Smooth-model inversion mathematically back-calculates (or “inverts”) the measured data to determine a subsurface resistivity structure. The results of the smooth-model inversion are intentionally gradational, rather than showing abrupt, blocky changes in the subsurface. The smooth-model algorithm includes accurate modeling of two-dimensional topography along with subsurface resistivity (MacInnes and Zonge, 1996).

These inversion results should not be considered a unique solution, and some ambiguity remains in any mathematical representation of the data. The inversion assumes a 2D earth with bodies having a significant lateral extent outside of the 2D cross-sectional plane. For 3D bodies this inversion will be in error. In addition, the ERT method will detect anomalies that are off-line or out of the plane from the transect but without the ability to determine where those out of plane anomalies originate.

Inversion output was saved as an ASCII format XYZ file containing position, elevation, and resistivity. The data were imported into Surfer mapping system where the resistivity models were

converted to a log format, gridded, contoured, and annotated for presentation. Results are presented as color cross sections showing the resistivity distribution derived from the smooth-model inversion process. Profile distance is shown across the base of the cross section, and elevation is labeled along the side. Additional masking of data along the edges of the cross-section is performed, beyond the limits of the geometric locations of the data points.

5 DISCUSSION OF RESULTS

The seismic models for this project are discussed below in a South to North order and presented as Figures 5-13. For ease of comparison and correlation, common horizontal and vertical scales (1:35) were used for SL-11 through SL-20. Due to the length of the lines, a different scale (1:70) was used for SL-41, SL-42, and SL-43. There is no vertical exaggeration for any of the presented models.

Tomographic seismic models are presented with the layer boundaries from the layer-based modeling superimposed as heavy cross-symbols. In tomographic models, sharp layer contacts are not clearly defined and thus ranges of velocities are used to interpret possible rock conditions and competency. A color scalebar is used to describe modeled velocities from the tomographic modeling process.

Tomographic inversion techniques will typically model a gradual increase in velocity with depth even if an abrupt velocity contact is present. Therefore, if velocity gradients are not present, tomographic inversion routines will overestimate and underestimate velocity above and below a layer contact, respectively. Velocity gradients can be very common in geologic environments with weathering zones and multiple types of rock, or areas with differential compaction and fill materials.

The color scheme used on the seismic tomography images is the same across profiles. The transition from blue to green occurs at a velocity of 950 ft/s and is commonly coincident with a refracting layer identified in the layer-based modeling scheme. Higher-velocity material, 1,600 – 2,000 ft/s (P-wave) is observed beneath the profiles at depth and apparently shallow beneath the southeast ends of the lines. These color ranges and apparent refractors may not mark a distinct geologic contact but are instead only indicators that a seismic velocity contrast is present. This could be a geologic contact but may be a result of differential weathering, compaction, cementation, etc. – factors that affect the overall density of the rock unit.

The electrical resistivity model SL-43 is presented on Figure 7. The color scheme used on the electrical resistivity images is a semi-log scale to enhance the contrast between high and low resistivities.

5.1 Seismic Refraction Line SL-41

SL-41 was collected on January 14. This line required three overlapping spreads to achieve the profile lengths of 950 feet. A 10-foot geophone spacing was used. This line was located on the shoulder of Highway 101 and had occasional access for use of the vehicle-mounted accelerated weight drop. This allowed for far off-end shots (100+ feet) and increased ability to identify deeper refractors.

The layer-based model for SL-41 (Figure 5) indicates a 900 ft/s layer overlying an intermediate layer with a modeled velocity of 5,500 ft/s that is interpreted as shallow saturated sediments (water table). A relatively fast layer (7,250 ft/s) layer is modeled 30-35 feet beneath the southern end of line, 100+ feet beneath the central portion of the line and 80+ feet beneath the northern

end of line. The tomographic model for SL-41 (Figure 5) smooths the contact between the saturated layer and interpreted medium-hard bedrock and shows lateral velocity variations along the line as well.

5.2 Seismic Refraction Line SL-42

SL-42 was collected on the afternoon of January 15 when noise levels from wave activity were significant. This line required two overlapping spreads to achieve the profile lengths of 710 feet. A 10-foot geophone spacing was used. There was no accessible space for the accelerated weight drop. Most of this line was located west of the embankment for the southbound lane, in high vegetation and very loose soils. Data quality was poor due to ocean wave noise, which would not have been overcome by the seismic sources available. Even explosive sources would have required “re-shoots” as the ocean wave noise occurred randomly and would wipe out weight shots on the other highway lines. Rather than pick noisy, data, an already subjective process, reliable picking of first arrivals was limited to the nearest ~24 channels, or less. Far off-end shots were not able to be used to identify deep bedrock refractors.

The tomographic model (Figure 6) indicates slow surface soils (625 ft/s) over a stiffer soil layer (2,060 ft/s) over a layer having P-wave velocity of ~4,975 ft/s, interpreted as the water table. The tomographic model implies faster material that would be consistent with the argillite rock at the depth limit of the central portion of the line (80+ feet) and shallower beneath the northern end of line (35-50 feet).

5.3 Seismic Refraction and Resistivity Line SL-43

SL-43 was collected in the morning hours of January 15. This line required three overlapping spreads to achieve the profile lengths of 950 feet. A 10-foot geophone spacing was used.

The layer-based model for SL-43 (Figure 7, top panel) indicates a layer having a velocity similar to or less than the air-wave (1,100 ft/s) overlying an intermediate layer with a modeled velocity of 4,700 ft/s that is interpreted as shallow saturated sediments (water table). A relatively fast layer (7,900 ft/s) layer is modeled 20-60 feet beneath most of the line. At the location of boring B-47, this correlates to rock identified as argillite. The tomographic model for SL-43 smooths the contact between the saturated layer and interpreted medium-hard bedrock and shows that bedrock may be deeper than 70-feet beneath the southern end of the line.

The electrical resistivity tomography model for SL-43 (Figure 7, bottom panel) generally correlates with the seismic refraction model. The surface soils are relatively resistive (350-400 ohm-m) compared to underlying layers. Beneath this, modeled resistivity values of less than 100 ohm-m imply saturated sediments or saturated weathered bedrock. The deeper refractor in the layer-based seismic model approximates a zone of relatively low resistivity (60 ohm-m). We do not expect that the resistivity survey penetrated this low-resistivity unit with strong enough returned signal to model deeper layers, though the apparent increase in resistivity at depth more indicate tighter, lower porosity rocks. A longer line, capable of imaging deeper, would help confirm this.

The seismic model indicates a thicker section of the second velocity layer, beneath the southern end of the line. The electrical model indicates thicker, more resistive materials at this location.

5.4 Seismic Refraction Line SL-11

SL-11 was collected in the morning of January 18. This line consisted of a single spread of 43 geophones spaced 6 feet apart for a total line length of 252 feet. There was no accessible space for far off-end shots (limited to approximately 50 feet beyond the ends of line). The 20-lb sledgehammer was the seismic source for the entirety of this line and data quality was excellent.

The layer-based model for SL-11 (Figure 8) indicates a thin surface soils layer with a velocity of 400 ft/s underlain by stiffer material with a velocity of 1,700 ft/s. This would be interpreted as a more consolidated soil layer. A relatively fast layer (7,425 ft/s) is 10-20 feet beneath the ground surface. The tomographic model for SL-11 (Figure 8) smooths the contacts between the bulk velocity units as expected, but the structural characteristics of the model are in good agreement with the layer-based model.

5.5 Seismic Refraction Line SL-12

SL-12 was collected in the afternoon of January 17. This line consisted of a single spread of 47 geophones spaced 6 feet apart for a total line length of 276 feet. There was no accessible space for off-end shots beyond the high end of the line, but approximately 55 feet was available beyond the southern end of the line. The 20-lb sledgehammer was the seismic source for the entirety of this line and data quality was good-excellent, though winds picked up in the late afternoon toward the end of shooting, degrading data quality.

The layer-based model for SL-12 (Figure 9) indicates a thin surface soils layer with a velocity of 400 ft/s underlain by material with a velocity of 4,950 ft/s that is interpreted as weathered bedrock, but the velocity range would also be consistent with saturated sediments. This velocity unit becomes increasingly thick toward the northern end line, up slope. A relatively hard, fast layer (9,650 ft/s) is 15 feet beneath the ground surface of the southern end of the line, 22 feet BGS at profile station 140 feet (center of line) and 65+ feet at the northern end of line (up slope).

The tomographic model for SL-12 (Figure 9) smooths the contacts between the bulk velocity units as expected, but with lateral changes in the velocity gradients. Beneath the southern half of the line, the velocity gradient is tighter between the moderate velocity unit and interpreted hard rock layers. As the bedrock layer diverges from the general trend in surface topography (profile station 150 feet to end of line) the gradient is broader. This may indicate the bedrock weathering profile is thicker beneath the northern half of the line and may be partially evident in the travel time data rather than obscured by a shallow water table.

5.6 Seismic Refraction Line SL-13A

SL-13A was collected mid-day on January 17. This line consisted of a single spread of 46 geophones spaced 5 feet apart for a total line length of 225 feet. For project consistency, this line is presented “South to North” referencing the labeled stake positions, even though SL-13A is more “West to East” trending.

There was no accessible space for off-end shots north of the line, though an 8-foot off-end shot was located beyond the southern end of line. The 20-lb sledgehammer was the seismic source for the entirety of this line. Data quality was fair-good. However, the line length and lack of accessibility for far off-end shots greatly restricted the achievable depth of investigation.

This line was difficult to model for several reasons. (1) the shallowest layer has an apparent velocity slower than the air-wave, but due to the line being shot on a slope, the air-wave is very dominant (2) the northern third of the line (station $x=160\text{ft}$ to EOL) is fairly steep (3) the inability to locate a far off-end source point beyond the northern end of line made determination of the lowest refractor very subjective.

Our layer-based model (Figure 10) shows a 2- / partial 3-layered velocity system. The intermediate layer of $\sim 4,950\text{ ft/s}$ is only observed beneath the northern two-thirds of the line. This is underlain by a layer with approximate $5,500\text{ ft/s}$ P-wave velocity that is interpreted as groundwater. This layer-based model would be consistent with a shallow landslide of materials, or more simply as sloping materials with moderate velocity P-wave velocities intersecting the groundwater surface (having higher P-wave velocity). The tomographic model (Figure 10) smooths the contact between the shallow soil layer and the interpreted groundwater unit, eliminating the pinch out though the velocity gradient is thicker beneath the northern end of line.

Profile station $x=112$ is the approximate intersection of SL-13A with SL-12 (profile station $x=210$). Due to sloping surface topography and apparent strike and dip we do not expect the refractor intercepts to correlate precisely but they are in good agreement. The deep bedrock refractor beneath SL-12 is too deep to image beneath SL-13A. The intermediate velocity layer for SL-13A matches that of SL-12.

5.7 Seismic Refraction Line SL-13B

SL-13B was collected in the morning of January 17. This line consisted of a single spread of 48 geophones spaced 4 feet apart for a total line length of 188 feet. For project consistency, this line is presented “South to North” referencing the labeled stake positions, even though SL-13B is more “West to East” trending.

There was no accessible space for off-end shots north of the line, and only enough for a 12-foot off-end shot beyond the southern end of line. The 20-lb sledgehammer was the seismic source for the entirety of this line. Data quality was fair-good. However, the line length and lack of accessibility for far off-end shots greatly restricted the achievable depth of investigation.

Line SL-13B was difficult to model for the same reasons as SL-13A. However, during the early processing phase of picking first arrivals, it was decided that we could not consistently pick around the air-wave arrival, and that the resulting model would show a first layer velocity of $1,100\text{ ft/s}$. A 3-layer system was fit to the data indicating a surface soils layer of 450 ft/s overlying a $1,400\text{ ft/s}$ layer over a refractor with a velocity of $2,900\text{ ft/s}$. The velocity of the lower refractors is very different than elsewhere on the project and may represent a different rock unit, or the entirety of the depth range of this profile be limited to soil over (very) weathered rock. No hard rock velocities are modeled beneath this line. The tomographic model (Figure 11) does fit a relatively higher-velocity zone to the travel time curves beneath the southern end of the

line. This zone would be parallel to the slope section of SL-13A and the velocity structure is in fair agreement between these two lines.

In order to properly characterize the bedrock geometry and weathering profile beneath SL-13A and SL-13B, the lines should be extended (receiver array at least 450 feet in length). Remote shot locations should be used, but with the limited accessible space this would require considerable effort.

5.8 Seismic Refraction Line SL-20

SL-17 was collected on January 16. This line consisted of a single spread of 46 geophones spaced 10 feet apart for a total line length of 450 feet. The northernmost geophone (geophone 46, at profile coordinate 450) was located in a very thick organic debris field (decomposed tree). We buried the geophone over 2 feet beneath the surface with no improvement to geophone coupling, and offset it from the linear profile, also without improvement. Off-end shots were located 100+ feet beyond the northern (high) end of line and 50 feet beyond the southern (low) end of line. The Betsy Seisgun was the seismic source for the entirety of this line and data quality was excellent.

The layer-based model for SL-20 (Figure 12) indicates a thin surface soils layer with a velocity of 900 ft/s, though this may have been contaminated by the air-wave and overestimated. This low-velocity unit is underlain by material with a velocity of 3,300 ft/s that is interpreted as weathered bedrock, but the velocity range would also be consistent with partially saturated sediments. A relatively hard, fast layer (8,100 ft/s) is 20-30 feet beneath this line.

The tomographic model for SL-20 (Figure 12) smooths the velocity model, showing more lateral contrast within the interpreted bedrock layer. The 5,500 ft/s contour (typical velocity of sound wave in water) follows the interpreted lower refractor from the layer-based model, though a high-velocity (8,000 ft/s) zone is present between profile stations x=220-330 that would suggest hard bedrock.

5.9 Seismic Refraction Line SL-17

SL-17 was collected on January 19. This line consisted of a single spread of 48 geophones spaced 8 feet apart for a total line length of 376 feet. Off-end shots were located 50 feet beyond the northern (high) end of line and 100 feet beyond the southern (low) end of line. The Betsy Seisgun was the seismic source for the entirety of this line and data quality was excellent.

The layer-based model for SL-17 (Figure 13) indicates a thin surface soils layer with a velocity of approximately 900 ft/s, though this may have been contaminated by the air-wave and overestimated. This low-velocity unit is underlain by material with a velocity of 2,650 ft/s that is interpreted as weathered bedrock or dense soil. A relatively hard, fast layer (9,200 ft/s) is 20-30 feet beneath the southern half of the line and becoming shallower to the north (15 feet BGS).

The tomographic model for SL-17 (Figure 13) indicates fairly tight velocity gradients between the velocity units identified in the layer-based model, implying the rock has a fairly thin or well-defined weathering zone.

5.10 Landslide Interpretation

The seismic survey does not appear to be capable of distinguishing between blocked landslide material and in-place native rock of the same type. Either (a) there is not enough of a velocity contrast to differentiate the two or (b) the contact between the two is deeper than the achieved depth of investigation.

The velocity data for B-50 (GEOVision PS Suspension Log data) does not indicate a clear velocity difference between various depth zones of the rock described in the preliminary boring logs as argillite. In general, bedrock velocity increases with depth, though there is some interbed variability as expected. The S-wave data for this borehole removes the complication of fluid contribution to velocity and indicates a fairly consistent seismic velocity in the upper 75 feet.

If the contact is deeper, it will be difficult to improve the refraction depth of investigation without the use of explosive energy sources. A very general rule of thumb is that the refraction array should be at least five times as long as the desired depth of investigation (ignoring geologic contribution). Due to this, longer receiver arrays are expected in the scope of work. For the energy to travel the length of long receiver arrays, larger seismic sources are necessary. On SL-20, the Betsy Seisgun was able to generate enough energy to pick first arrivals 500+ feet away from the shot, but this should not be expected for lines collected near the highway. While shots could be timed during paused traffic, random wave action would result in many discarded shots.

Resistivity tomography has similar “rule of thumb” depth estimates as seismic refraction (again, without considering geology). Instead of combating ambient seismic noise, the difficulty would be getting strong signal returned through the shallow, conductive materials below the water table. The GEOVision dual induction log for B-50 indicates the rock resistivity ranges between 50–100-ohm meters, which is relatively conductive. This is corroborated with the resistivity data collected along SL-43. The resistivity array may be customized to potentially image as deep as 200 feet beneath a 1000-foot-long line if a strong signal is returned.

6 CERTIFICATION

All geophysical data, analysis, interpretations, conclusions, and recommendations in this document have been prepared under the supervision of and reviewed by a **GEOVision** California Professional Geophysicist.

Prepared by,



03/12/2021

Christopher Martinez
Staff Geophysicist
GEOVision Geophysical Services

Date

and



03/12/2021

J.B. Shawver
Geophysicist
GEOVision Geophysical Services

Date

- * This geophysical investigation was conducted under the supervision of a California Professional Geophysicist using industry standard methods and equipment. A high degree of professionalism was maintained during all aspects of the project from the field investigation and data acquisition, through data processing, interpretation, and reporting. All original field data files, field notes, observations, and other pertinent information are maintained in the project files and are available for the client to review for a period of at least one year.

A professional geophysicist's certification of interpreted geophysical conditions comprises a declaration of his/her professional judgment. It does not constitute a warranty or guarantee, expressed or implied, nor does it relieve any other party of its responsibility to abide by contract documents, applicable codes, standards, regulations, or ordinances.

7 REFERENCES

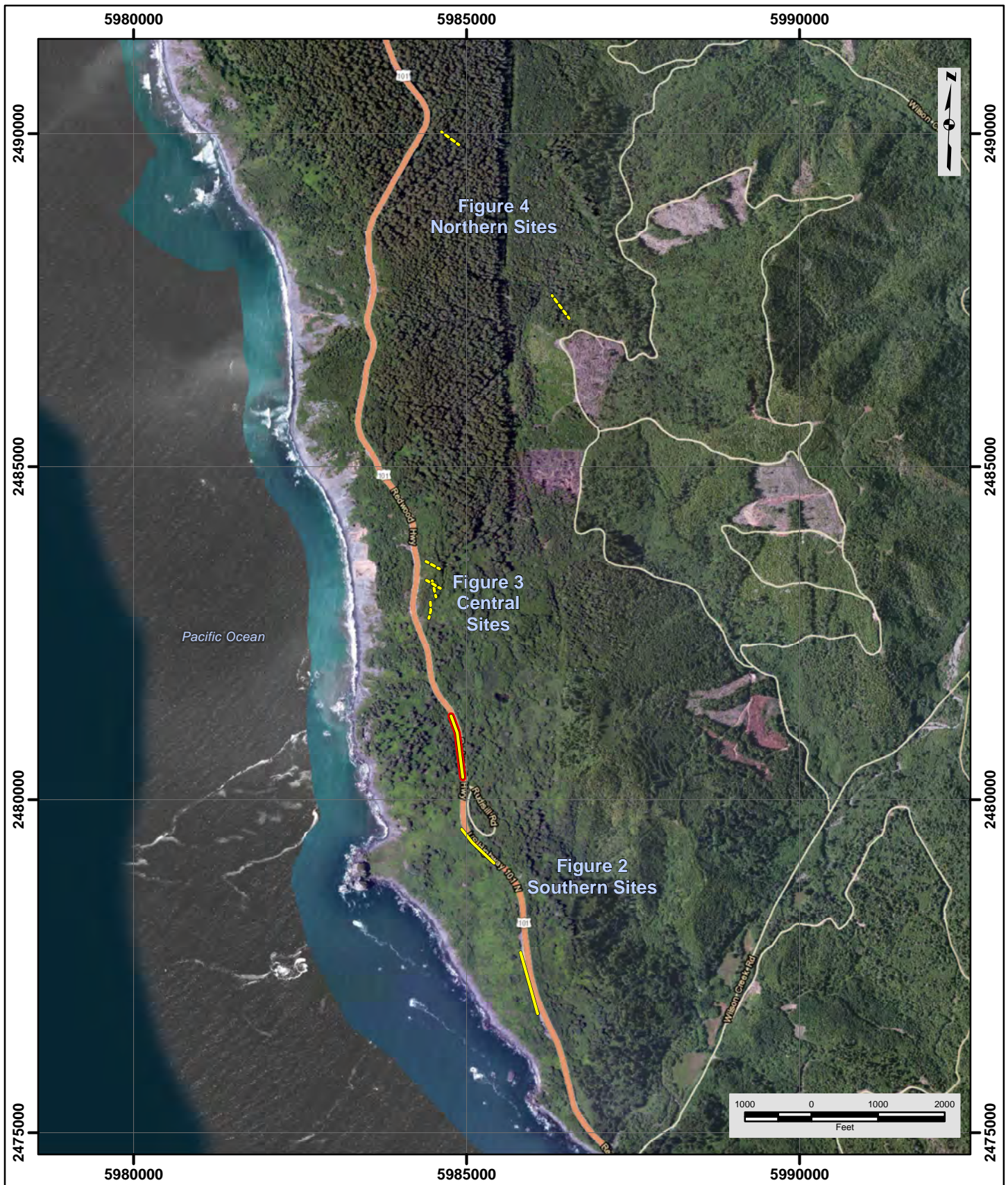
- Ali Ak, M., 1990, An Analytical Raypath Approach to the Refraction Wavefront Method, *Geophysical Prospecting*, Volume 38, 971-982.
- ASTM Standard Guide D5777 - 18, Standard Guide for Using the Seismic Refraction Method for Subsurface Investigation, ASTM International, West Conshohocken, PA, 2018, www.astm.org.
- ASTM D6431-18, Standard Guide for Using the Direct Current Resistivity Method for Subsurface Investigation, ASTM International, West Conshohocken, PA, 2010, www.astm.org
- Dahlin, T., 1996, 2D Resistivity Surveying for Environmental and Engineering Applications, *First Break*, v14, p275-283.
- Delattre, M., and Rosinski, A., 2012, Preliminary Geologic Map of the Onshore Portions of the Crescent City and Orick 30' x 60' Quadrangles, California, California Geological Survey
- Dobrin, M.S., and Savit, J., 1988, *Introduction to Geophysical Prospecting*, McGraw-Hill Co., New York.
- Edwards, L.S., 1977, A Modified Pseudosection for Resistivity and IP: *Geophysics*, v42, p1020-1036.
- GEOVision, 2021, Report 20020-02 Rev 0, Last Chance Grade Borehole Geophysics Crescent City, California, Prepared for HNTB Corporation, dated March 2021.
- Kearey, P., and Brooks, M., 1991, *An Introduction to Geophysical Exploration*, Second Edition, Blackwell Science, Ltd., Osney Mead, Oxford
- Lankston, R. W., 1990, High-resolution refraction seismic data acquisition and interpretation, *in* Ward, S. H., ed., *Geotechnical and Environmental Geophysics, Volume I: Review and Tutorial*: Society of Exploration Geophysicists, Tulsa, Oklahoma, p. 45-74.
- Loke, M.H., and Barker, R.D., 1996, Rapid Least-Squares Inversion of Apparent Resistivity Pseudosections by a Quasi-Newton method: *Geophysical Prospecting*, v44, 131-152.
- MacInnes, Scott and Zonge, Ken, 1996, 2D Inversion of Resistivity and IP Data with Topography, *Proceedings of the Northwest Mining Association, 102nd Annual Convention*, Spokane, Washington, 1996.
- Oldenburg, D. W. and Li, Y., 1999, Estimating Depth of Investigation in DC resistivity and IP surveys, *Geophysics*, 64. 403-416.
- Palmer, D. 1981, An Introduction to the Generalized Reciprocal Method of Seismic Refraction Interpretation. *GEOPHYSICS*, 46(11), 1508–1518.
- Redpath, B. B., 1973, Seismic refraction exploration for engineering site investigations: U. S. Army Engineer Waterway Experiment Station Explosive Excavation Research Laboratory, Livermore, California, Technical Report E-73-4, 51 p.
- Rohdewald, S., 2011, Interpretation of First-Arrival Times with Wavefront Eikonal Traveltime Inversion and Wavefront Refraction Method, *In Proceedings of the 2011 Annual Symposium on the Application of Geophysics to Engineering and Environmental Problems*
- Telford, W. M., Geldart, L.P., Sheriff, R.E., 1990, *Applied Geophysics*, Second Edition, Cambridge University Press.
- Wills, C.J., 2000, Landslides in the highway 101 corridor between Wilson Creek and Crescent City, Del Norte County, California: California Geological Survey, Special Report 184, 24 p., map scale 1:24,000

8 TABLES AND FIGURES

Name	Label	Location	Profile Distance (feet)	Northing	Easting
				(US Survey feet)	
11-1	11-Start	South	0	2482723.0	5984431.3
11-22	11-Bend		60	2482841.9	5984460.8
11-43	11-End	North	252	2482965.3	5984454.5
12-1	12-Start	South	0	2483043.7	5984537.6
12-48	12-End	North	276	2483311.9	5984476.8
13A-1	13A-Start	South	0	2483168.5	5984609.7
13A-46	13A-End	North	225	2483294.1	5984396.3
13B-1	13B-Start	South	0	2483465.4	5984590.6
13B-46	13B-End	North	188	2483577.6	5984389.8
17-1	17-Start	South	0	2489831.4	5984880.3
17-46	17-End	North	376	2490026.0	5984622.8
20-1	20-Start	South	0	2487226.1	5986537.8
20-46	20-End	North	450	2487568.1	5986282.4
41-1	41-Start	South	0	2476786.0	5986066.2
41-97	41-End	North	960	2477705.4	5985809.7
42-1	42-Start	South	0	2479047.1	5985413.2
42-46	42-Bend		450	2479355.7	5985086.7
42-72	42-End	North	710	2479556.2	5984926.0
43-1	43-Start	South	0	2480331.0	5984942.2
43-69	43-Bend		680	2481004.0	5984859.5
43-96	43-End	North	950	2481255.9	5984764.4

Table 1: Geophysical Line Geometry

Coordinates system: California State Plane Zone 1, US Survey Feet, North American Datum 1983



- Location of Seismic Refraction Line
- Approximate Location of Seismic Refraction Line
- Location of Electrical Resistivity Line

NOTES:

1. Coordinate System: California State Plane, NAD83, Zone I (0401), US Survey Feet
2. Base map source: Esri, DigitalGlobe, GeoEye, Earthstar Geographics, CNES/Airbus DS, USDA, USGS, AeroGRID, IGN, and the GIS User Community

Date: 1/29/2021

GV Project: 20020

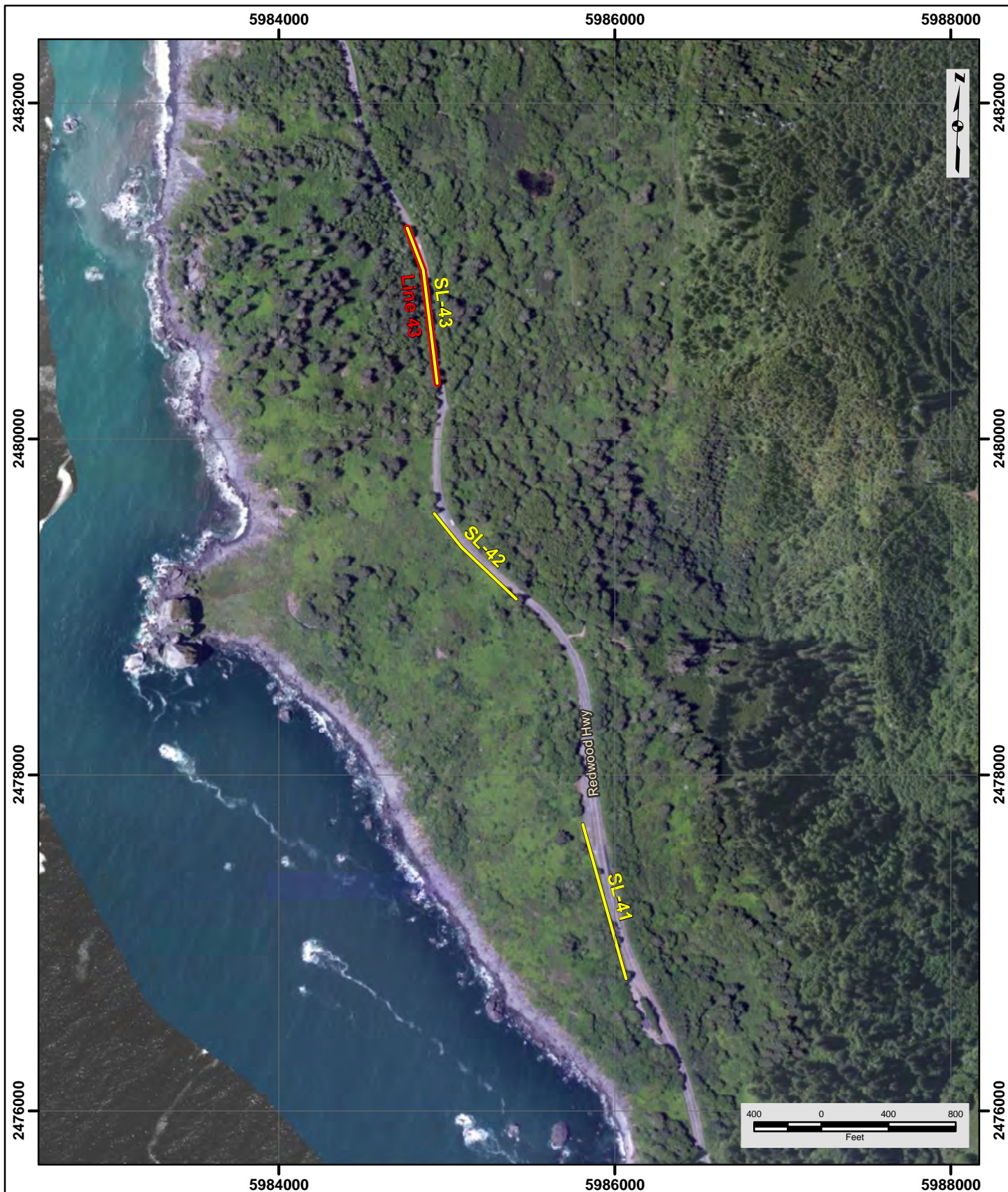
Developed by: C Martinez

Drawn by: T Rodriguez

Approved by: J Shawver

File Name: 20020-1.MXD

FIGURE 1 SITE LOCATION MAP
LAST CHANCE GRADE PROJECT DEL NORTE COUNTY, CALIFORNIA
PREPARED FOR HNTB CORPORATION



- Location of Seismic Refraction Line
- Location of Electrical Resistivity Line

NOTES:

1. Coordinate System: California State Plane, NAD83, Zone 1 (0401), US Survey Feet
2. Base map source: Esri, DigitalGlobe, GeoEye, Earthstar Geographics, CNES/Airbus DS, USDA, USGS, AeroGRID, IGN, and the GIS User Community

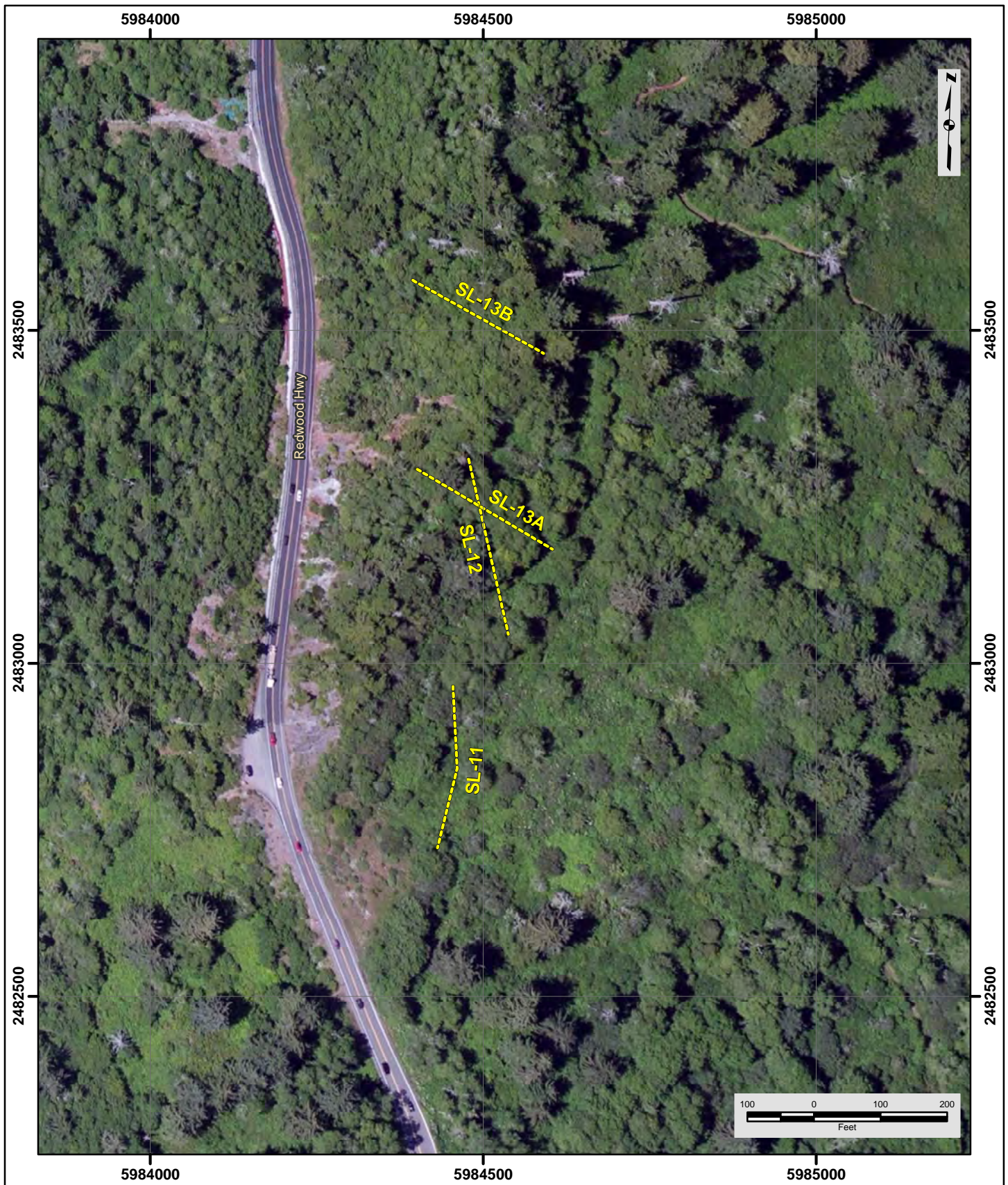



Date: 1/29/2021
 GV Project: 20020
 Developed by: C Martinez
 Drawn by: T Rodriguez
 Approved by: J Shawver
 File Name: 20020-2.MXD

**FIGURE 2
SITE MAP**

**LAST CHANCE GRADE PROJECT
SOUTHERN SURVEY LOCATIONS
DEL NORTE COUNTY, CALIFORNIA**

**PREPARED FOR
HNTB CORPORATION**



 Approximate Location of Seismic Refraction Line

NOTES:

1. Coordinate System: California State Plane, NAD83, Zone I (0401), US Survey Feet
2. Base map source: Esri, DigitalGlobe, GeoEye, Earthstar Geographics, CNES/Airbus DS, USDA, USGS, AeroGRID, IGN, and the GIS User Community

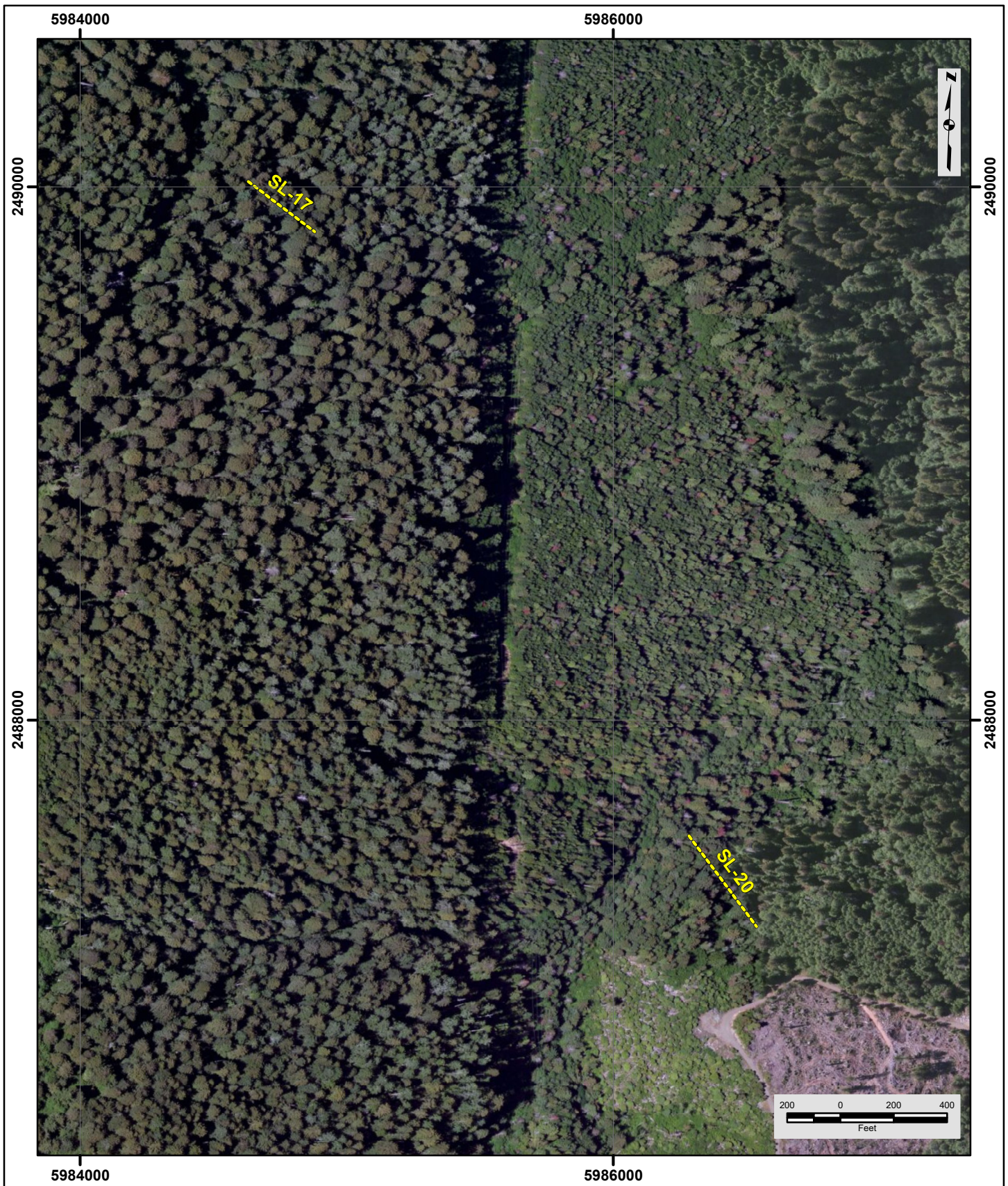


Date:	1/29/2021
GV Project:	20020
Developed by:	C Martinez
Drawn by:	T Rodriguez
Approved by:	J Shawver
File Name:	20020-3.MXD

**FIGURE 3
SITE MAP**

**LAST CHANCE GRADE PROJECT
CENTRAL SURVEY LOCATIONS
DEL NORTE COUNTY, CALIFORNIA**

**PREPARED FOR
HNTB CORPORATION**



 Approximate Location of Seismic Refraction Line

NOTES:

1. Coordinate System: California State Plane, NAD83, Zone 1 (0401), US Survey Feet
2. Base map source: Esri, DigitalGlobe, GeoEye, Earthstar Geographics, CNES/Airbus DS, USDA, USGS, AeroGRID, IGN, and the GIS User Community

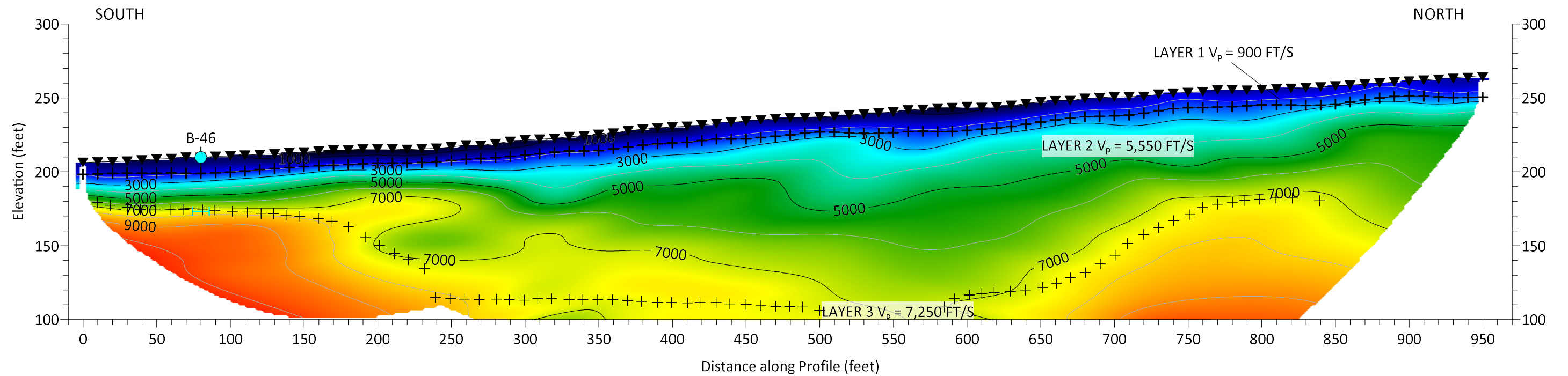
GEOVision
geophysical services

Date:	1/29/2021
GV Project:	20020
Developed by:	C Martinez
Drawn by:	T Rodriguez
Approved by:	J Shawver
File Name:	20020-4.MXD

**FIGURE 4
SITE MAP**

**LAST CHANCE GRADE PROJECT
NORTHERN SURVEY LOCATIONS
DEL NORTE COUNTY, CALIFORNIA**

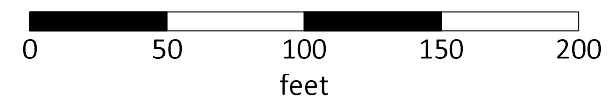
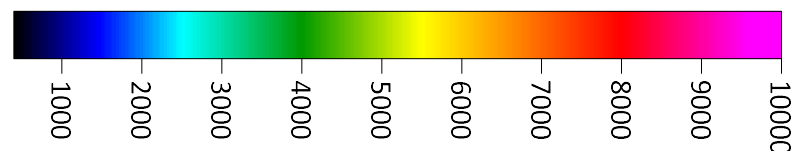
**PREPARED FOR
HNTB CORPORATION**



LEGEND

- ▼ Geophone / Electrode Location
- ⊕ Layer-Based Modeling Velocity Contact
- ◆ Borehole Location (projected)
- ⊢ Borehole Data / Contact

P-Wave Velocity (ft/s)

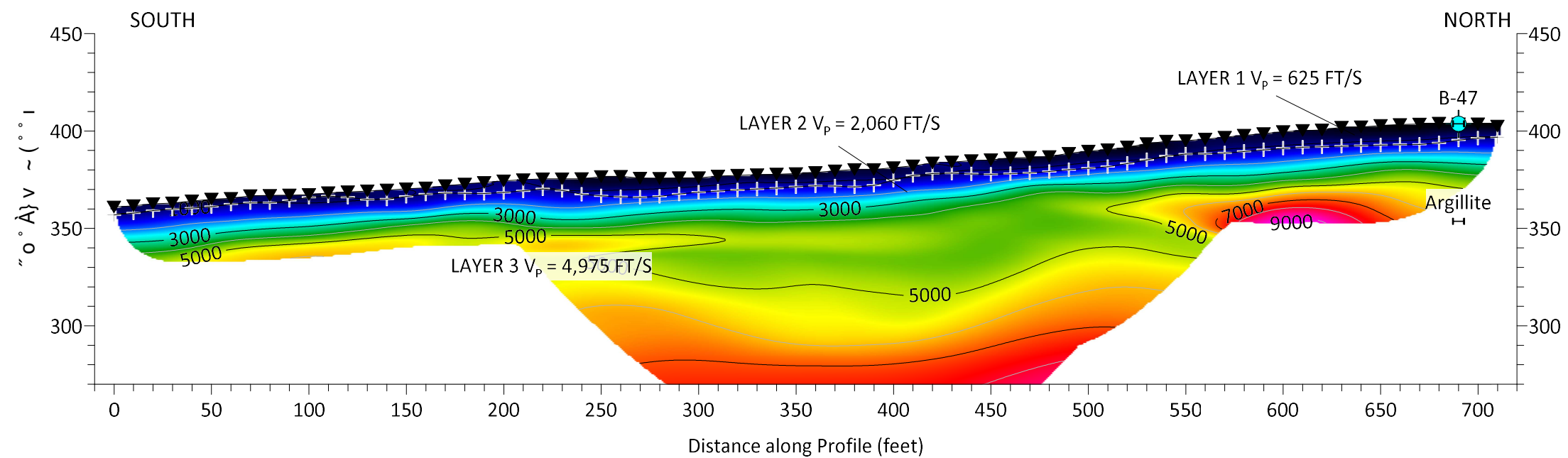


GEOVision
geophysical services

FIGURE 5

LINE SL-41
SEISMIC REFRACTION MODEL

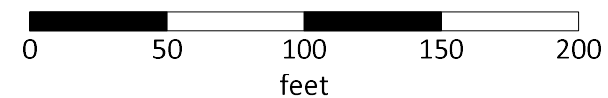
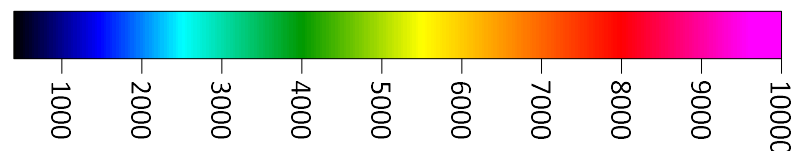
PREPARED FOR
HNTB CORPORATION



LEGEND

- ▼ Geophone / Electrode Location
- ⊕ Layer-Based Modeling Velocity Contact
- ◆ Borehole Location (projected)
- ⊢ Borehole Data / Contact
- ◆ Seismic Line Intercept

P-Wave Velocity (ft/s)

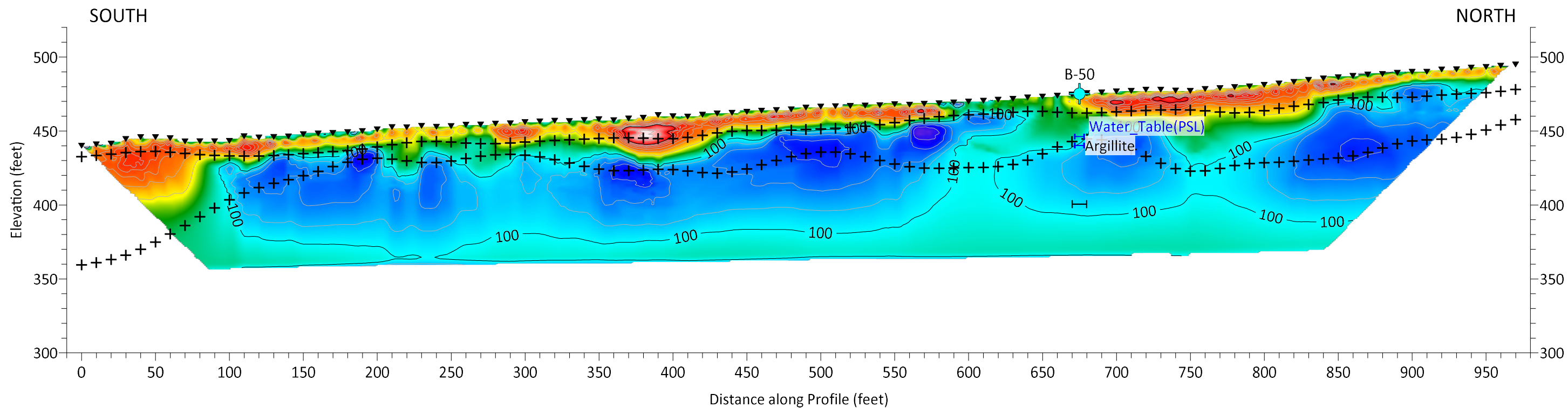
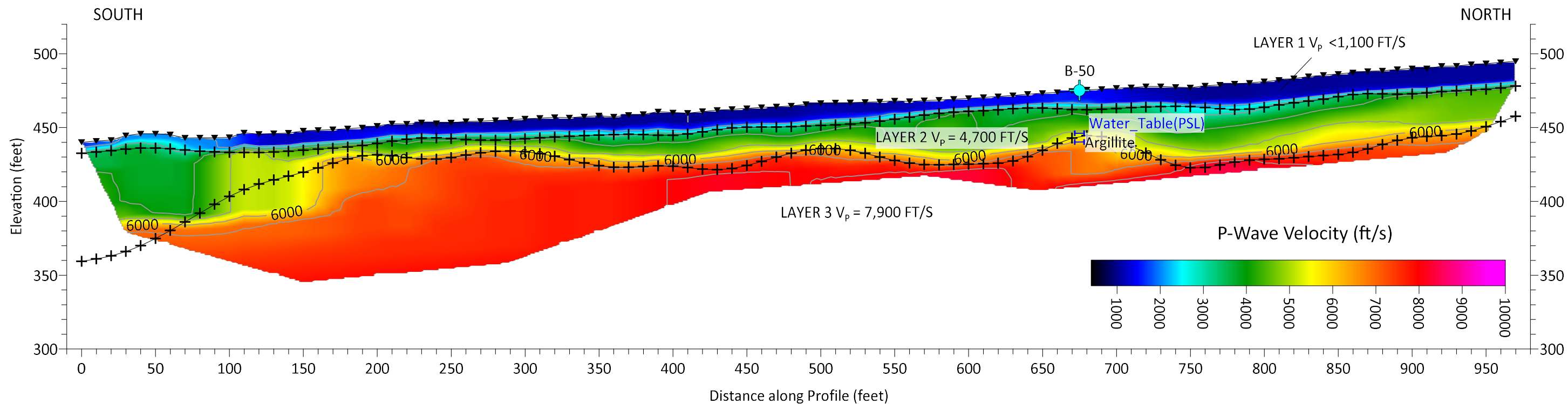


GEOVision
geophysical services

FIGURE 6

LINE SL-42
SEISMIC REFRACTION MODEL

PREPARED FOR
HNTB CORPORATION



LEGEND

- ▼ Geophone / Electrode Location
- ⊕ Layer-Based Modeling Velocity Contact
- ◆ Borehole Location (projected)
- ⊢ Borehole Data / Contact
- ◆ Seismic Line Intercept

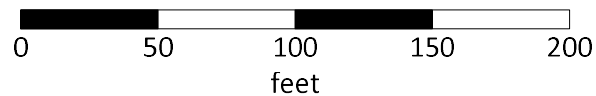
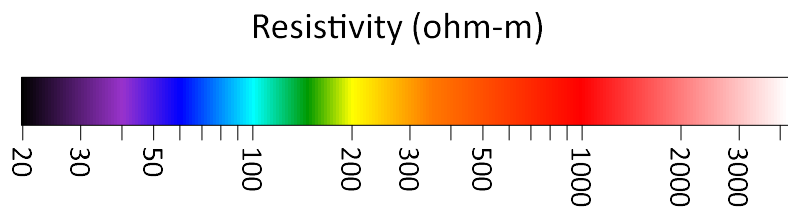
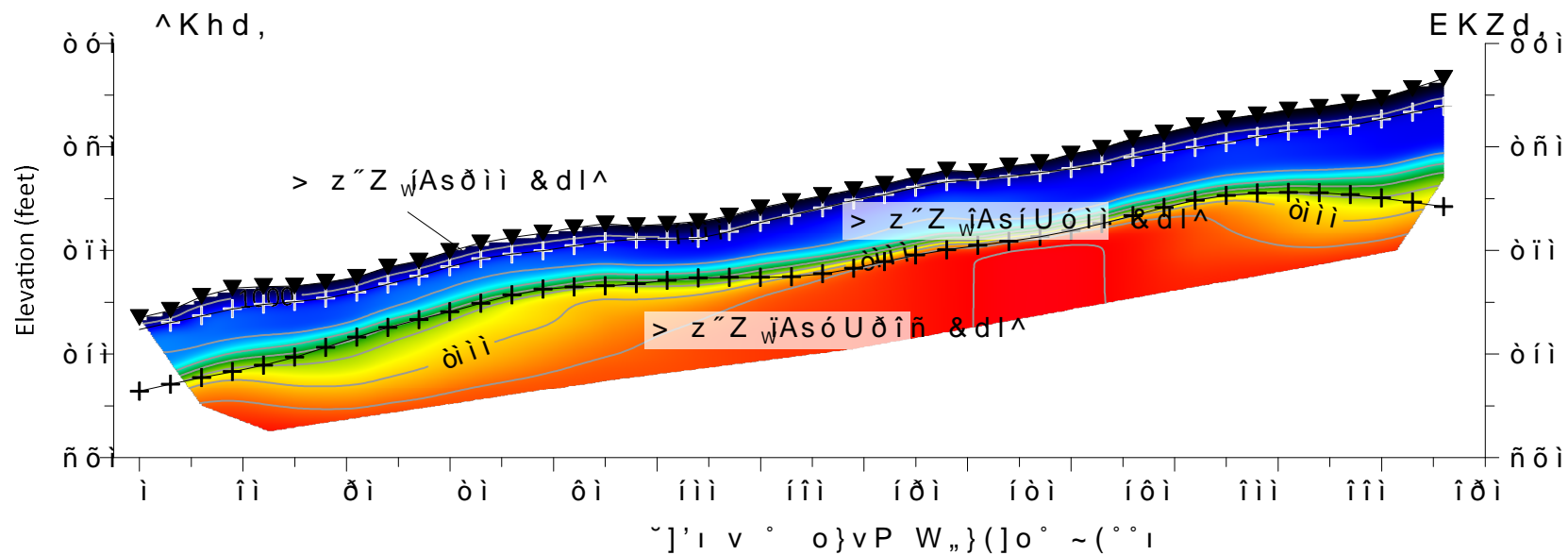


FIGURE 7

LINE SL-43
SEISMIC REFRACTION &
ELECTRICAL RESISTIVITY MODELS

PREPARED FOR
HNTB CORPORATION



LEGEND

▼

Geophone / Electrode Location

+

Layer-Based Modeling Velocity Contact

◆

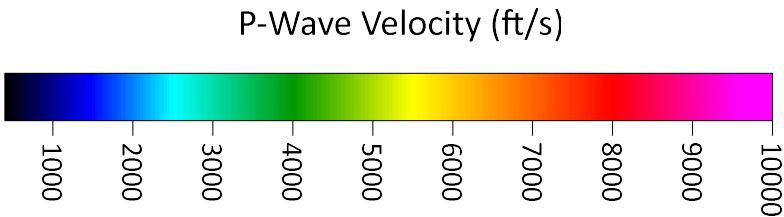
Borehole Location (projected)

—

Borehole Data / Contact

◆

Seismic Line Intercept



GEO

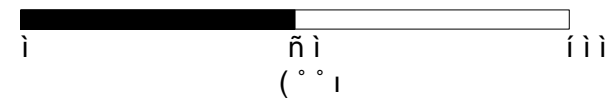
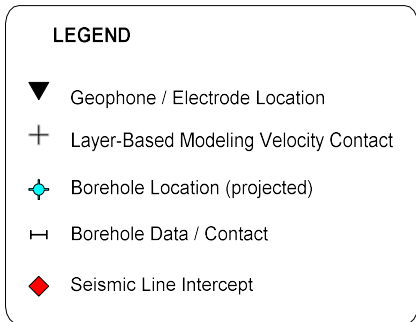
Vision

geophysical services

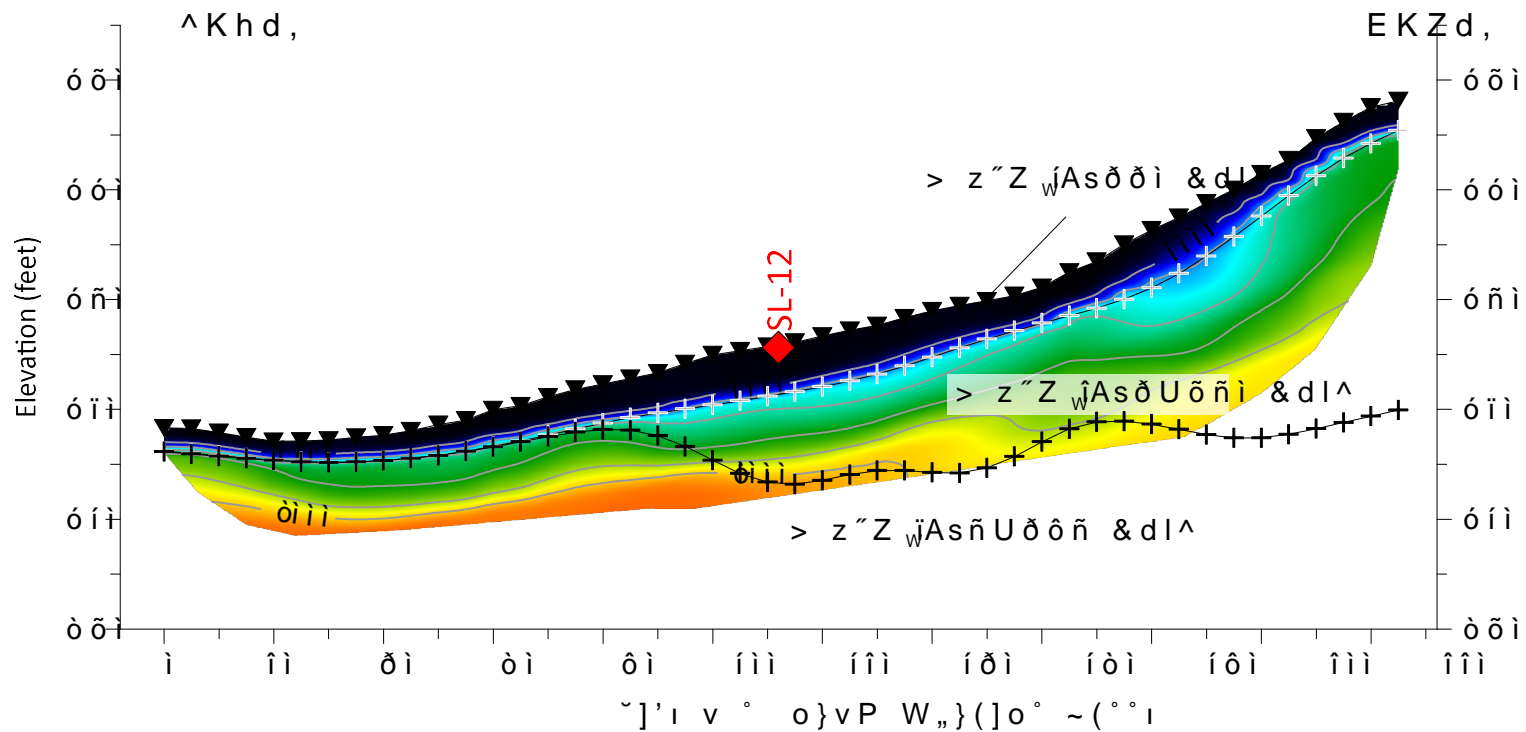
FIGURE 8

LINE SL-11
SEISMIC REFRACTION MODEL

PREPARED FOR
HNTB CORPORATION



PREPARED FOR
HNTB CORPORATION



LEGEND

▼

Geophone / Electrode Location

+

Layer-Based Modeling Velocity Contact

◆

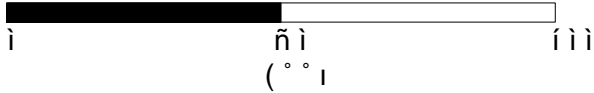
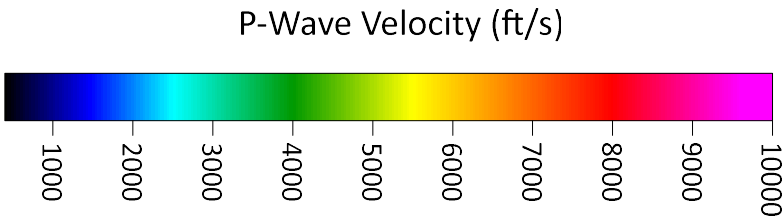
Borehole Location (projected)

⊢

Borehole Data / Contact

◆

Seismic Line Intercept



GEO

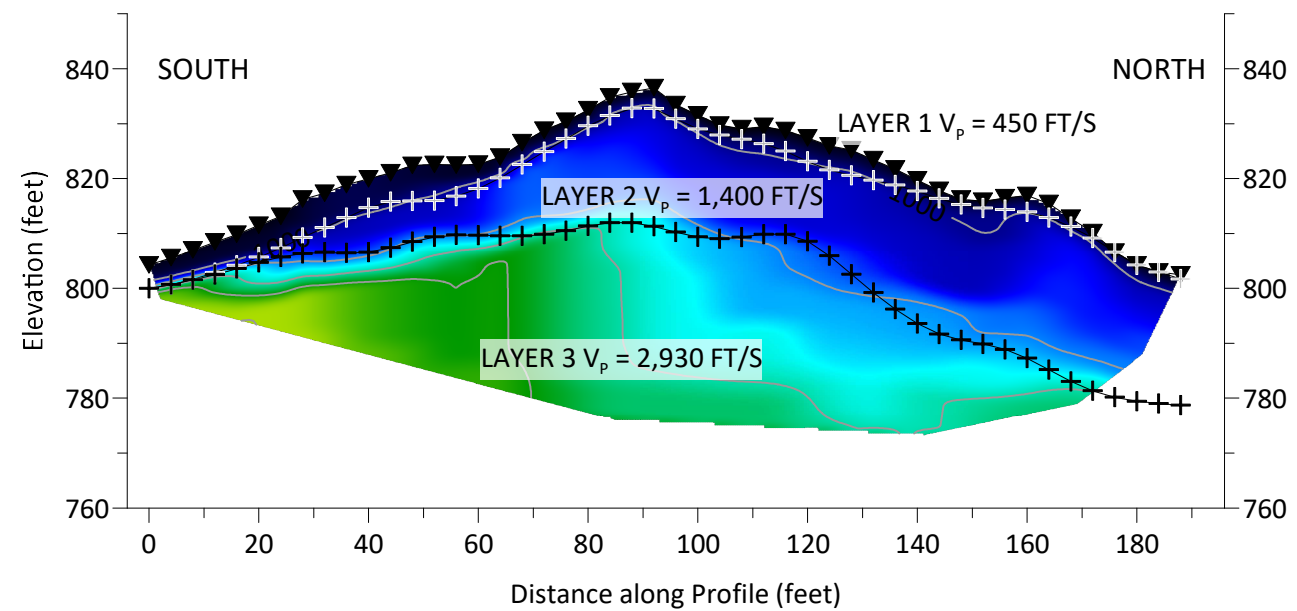
Vision

geophysical services

FIGURE 10

LINE SL-13A
SEISMIC REFRACTION MODEL

PREPARED FOR
HNTB CORPORATION



LEGEND

▼

Geophone / Electrode Location

+

Layer-Based Modeling Velocity Contact

◆

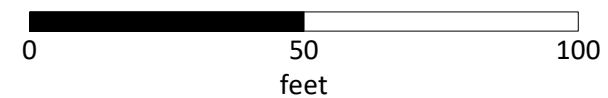
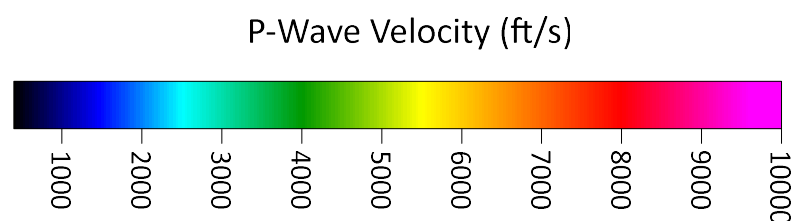
Borehole Location (projected)

⊢

Borehole Data / Contact

◆

Seismic Line Intercept



GEO

Vision

geophysical services

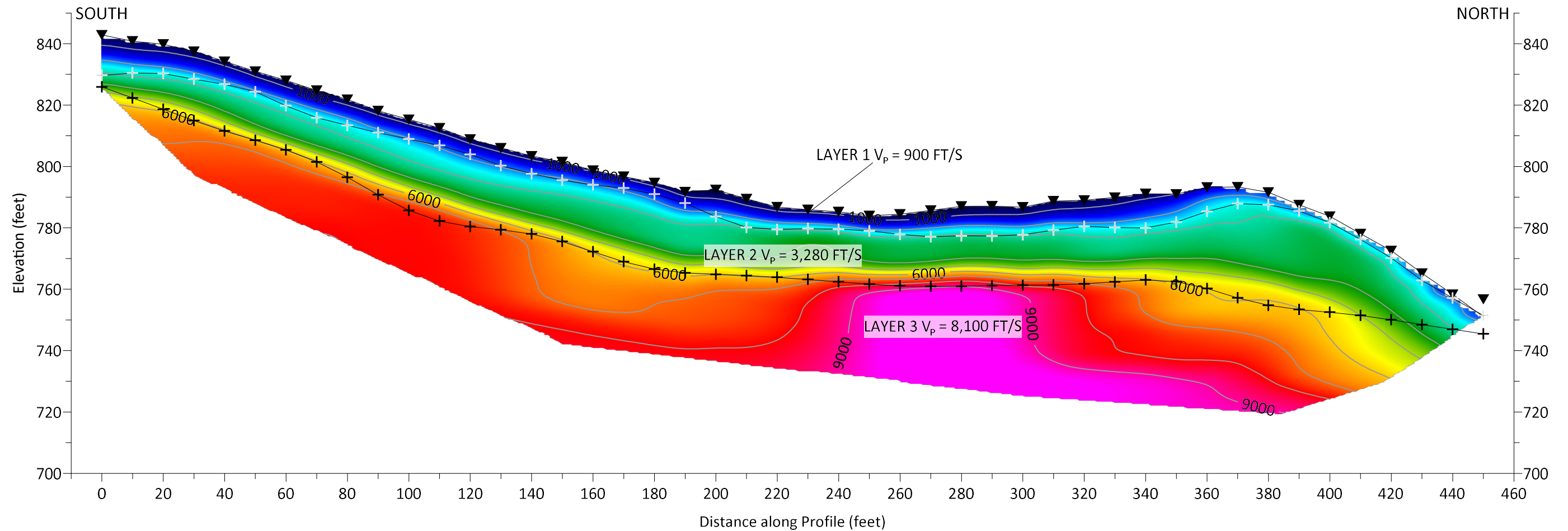
FIGURE 11

LINE SL-13B

SEISMIC REFRACTION MODEL

PREPARED FOR

HNTB CORPORATION



LEGEND

- ▼ Geophone / Electrode Location
- ⊕ Layer-Based Modeling Velocity Contact
- ◆ Borehole Location (projected)
- ⊢ Borehole Data / Contact
- ◆ Seismic Line Intercept

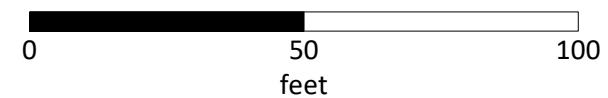
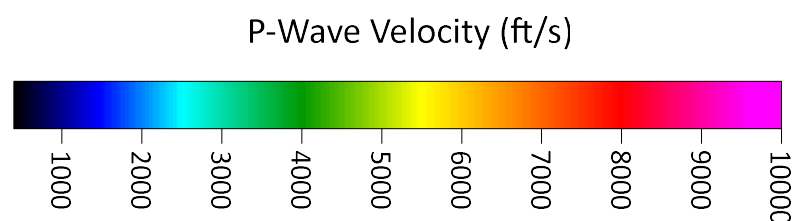
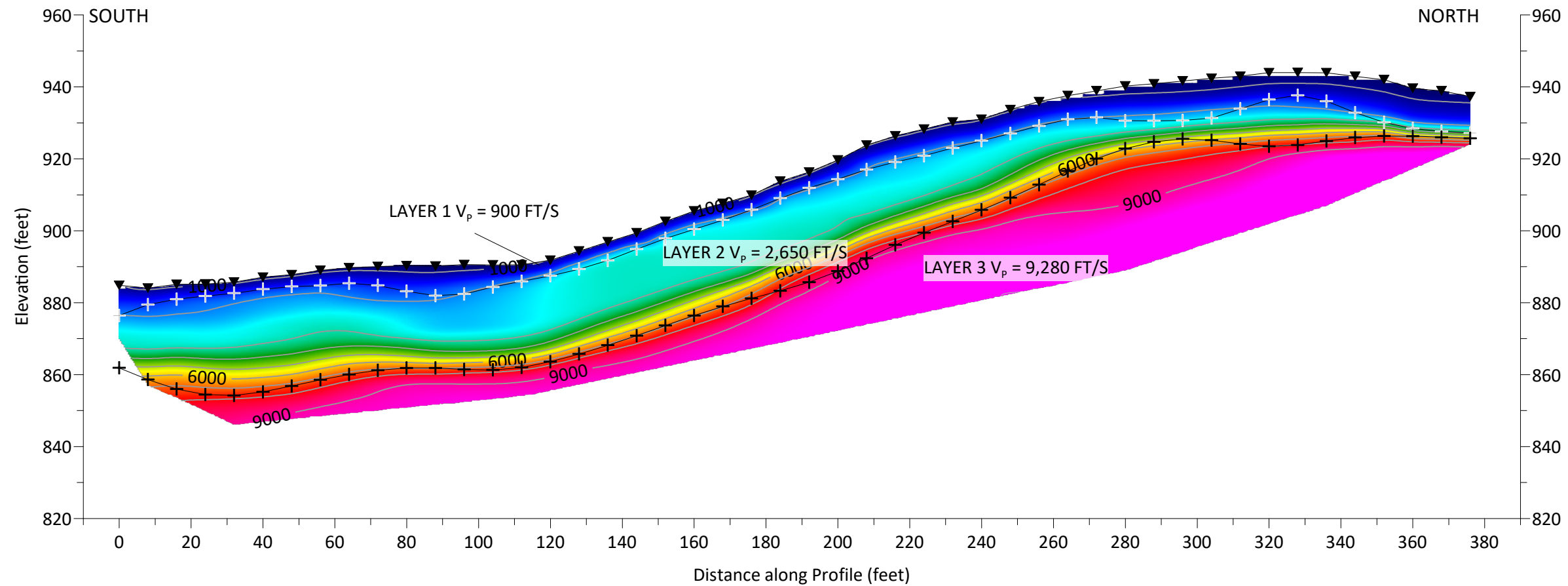


	FIGURE 12
	LINE SL-20 SEISMIC REFRACTION MODEL
	PREPARED FOR HNTB CORPORATION



LEGEND

- ▼ Geophone / Electrode Location
- ⊕ Layer-Based Modeling Velocity Contact
- ◆ Borehole Location (projected)
- ⊢ Borehole Data / Contact
- ◆ Seismic Line Intercept

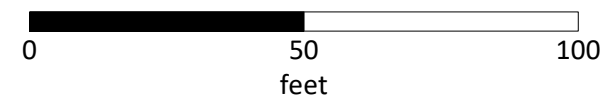
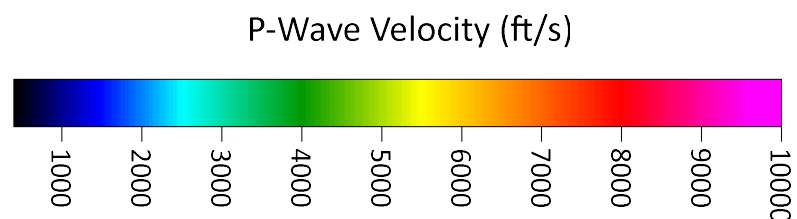


FIGURE 13

LINE SL-17
SEISMIC REFRACTION MODEL

PREPARED FOR
HNTB CORPORATION